Active Control of Rotor Supported by Faulting Journal Bearing

Matheus Freire Wu(✉), Tiago Henrique Machado, and Katia Lucchesi Cavalca

Faculty of Mechanical Engineering, University of Campinas, Campinas, Brazil
{matheusfw, tiagomh, katia}@fem.unicamp.br

Abstract. Although hydrodynamic bearings have minimum contact between solid parts, under particular circumstances they might be susceptible to abrasion and wear. In order to mitigate the problem, it is proposed to apply active control methods to reduce the vibration level at critical situations: fluid induced instability and the first bending mode. However, damage in the bearing surface have direct influence over the oil-film pressure and, consequently, in the bearings equivalent coefficients. Although, initially, small variations may lead to minor performance loss, when it becomes more significant close-loop stability may be affected. Therefore, in this paper it is conducted a preliminary study on the effect of journal bearing wear depth effects in active controlled rotors. A structured uncertain model is proposed to include the possible fault coefficients in the model allowing to perform robust stability analysis. Based on the uncertain formulation a robust control solution is designed guaranteeing rotor stability for a certain damage range.

Keywords: Robust control · Hydrodynamic journal bearing
Bearing wear damage

1 Introduction

During field operation every machine component is susceptible to wear, which, in the beginning, causes small changes in the system behavior, but in the absence of maintenance, eventually, can lead to failure. It is not different for hydrodynamic journal bearing. Although the oil film provides isolation between solid parts minimizing friction during operation, when the shaft comes to a full stop there is direct contact with the bearing. When starting-up there may occur abrasion of the bearing surface, generally made of materials softer than the shaft. Contact between solid parts is also possible in cases of extreme vibration amplitudes, which may occur due to operation at critical speed, or at fluid induced instability condition.

Detection, analysis and modeling the effects of journal bearing wear is a challenging task. Over the years, several researchers have studied the stability of a worn bearing, as well as evaluated its performance under different circumstances [1–4]. Considerable research has also been carried out for the development of various techniques for bearing fault detection and diagnosis. As described by Machado et al. [5], these techniques can be mainly classified into two categories: time domain [6–8] and frequency domain techniques [9, 10].

K. L. Cavalca and H. I. Weber (Eds.): IFToMM 2018, MMS 62, pp. 49–64, 2019.
https://doi.org/10.1007/978-3-319-99270-9_4

Considering a rotor supported by hydrodynamic bearings susceptible to wear, the goal of this paper is to analyze those effects in an active controlled rotor and design an auxiliary robust active controller that allows to mitigate the possibilities for the damage propagation by reducing the vibration at critical speed and stabilizing the system at fluid induced instability. With active control, the rotor should be able to sustain safe operation levels until further scheduled maintenance to repair the damaged component.

The control force is supposed to act in the system via a magnetic actuator with the sole objective of controlling the vibration, all the rotor load should still be supported by the journal bearings. Applying the magnetic actuator only as an auxiliary component requires less powerful magnets which can significantly reduce the cost, size and energy consumption of the system. Many studies regarding active rotor vibration control can be found in literature, such as [11–17]. Studies focused on controlling fluid-induced instability can be found in the works [18–20]. Other significant contributions can be found in studies regarding levitating active magnetic bearings (AMB) [21–23]. However, most of the literature is concerned to the main source of parametrical variation, the rotational speed, which has direct influence over gyroscopic effect and journal bearing parameters. Few references concerning controlling damaged rotors can be found, being mostly related to levitating AMB under critical failure such as sensor or coils malfunctioning [24, 25].

Here it is proposed to design and compare, via numerical simulation, two different active control methods to be applied in a rotor supported hydrodynamic bearing evaluating the effect of abrasion damage on the close-loop performance. Both are static gain-scheduled controllers obtained by solving the two-stage method proposed in [26], but one considers uncertainties due to bearing wear in its project. The general guideline of this paper starts with the presentation of the rotor and its modeling, followed by a brief description of worn journal bearing coefficients modeling. Then, in Sect. 2, it is presented the approximation used to create a model fitted for the LMI formulation. In Sect. 3 is described the main formulation for the controllers and uncertainties. Finally, in Sects. 4 and 5 are the main results, discussion and conclusions.

2 Rotor Modeling

2.1 Rotor

For this study, the adopted rotor, Fig. 1, consists in a steel (SAE 1030) shaft of 583 mm length and 12 mm diameter bi-supported by hydrodynamic journal bearings, with the wear effect acting over the bearing number 2. Nominally, both bearings have 18 mm length, 31 mm diameter and radial clearance of 90 μm, and are lubricated by ISO VG 32 oil. The other main components are the disc with 47.5 mm length and 95 mm diameter, which adds load and it is the main source of unbalance to the system, and the journal with 80 mm length and 40 mm diameter through which a magnetic actuator applies the control force. For control feedback are considered the displacements of the bearings nodes at Y and Z directions. This configuration presents its first critical speed at about 46 Hz, and fluid induced instability near 79 Hz. To analyze the most important operational conditions, it is considered the rotor operational speed

range between 20 Hz and 100 Hz spanning the situations: before, at and after the critical speed, and above the fluid-instability threshold.

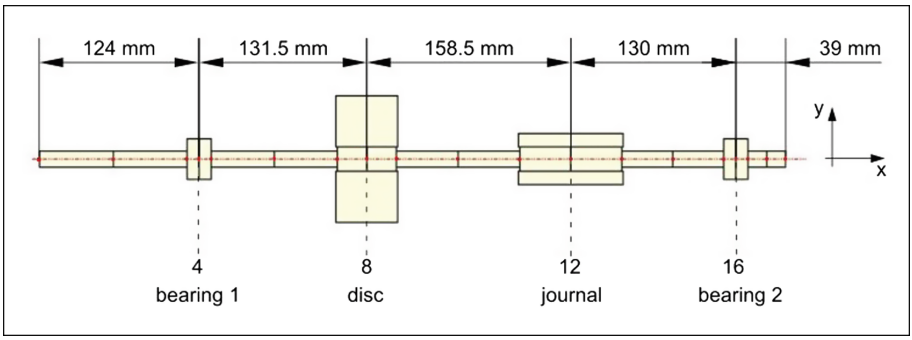

Fig. 1. Rotor FEM model, and main components and respective nodes.

The system is formulated following the finite element model (FEM) by Nelson [27], which allows to represent the set composed by the shaft, disc and journal as the classic second order equation of motion, Eq. (1), where $\mathbf{M_{fem}}$, $\mathbf{D_{fem}}$, $\mathbf{K_{fem}}$ and $\mathbf{G_{fem}}$ are respectively the global mass, damping, stiffness and gyroscopic matrices, $\boldsymbol{\Omega}$ is the system rotational speed, and $\mathbf{q}$ and $\mathbf{f}$ are respectively the degrees of freedom (DOF) and external excitation vectors.

$$\mathbf{M_{fem}}\ddot{\mathbf{q}} + (\mathbf{D_{fem}} + \Omega\mathbf{G_{fem}})\dot{\mathbf{q}} + \mathbf{K_{fem}}\mathbf{q} = \mathbf{f}(t) \tag{1}$$

2.2 Bearing and Wear Models

For the cylindrical journal bearings, it is used the approach of equivalent linear coefficients of stiffness and damping, which are inserted in the finite element model in bearing position. The procedure for obtaining these coefficients is based on the solution of Reynolds equation, the basis of hydrodynamic lubrication theory. The solution of Reynolds equation gives the pressure field generated by the oil film, and the hydrodynamic forces supporting the rotor are obtained by integration of this pressure around the shaft circumference. These general nonlinear hydrodynamic forces are then expanded into a Taylor series and the resulting differential expressions are approximated by finite differences in order to calculate the bearing equivalent coefficients of stiffness and damping, as shown in Eq. (2), as an example, for the cross coupled stiffness coefficient (K_{yz}) and damping coefficient (C_{zy}). Δz and $\Delta\dot{y}$ are, respectively, small perturbations in the shaft equilibrium position for displacement and velocity.

$$K_{yz} = \frac{\partial F_y}{\partial z} = \frac{\Delta F_y}{\Delta \bar{z}} \qquad C_{zy} = \frac{\partial F_z}{\partial \dot{y}} = \frac{\Delta F_z}{\Delta \dot{\bar{y}}} \tag{2}$$

For the numerical procedure to solve Reynolds equation, in the case when the oil-film thickness is discontinuous, it is used the approach presented by Machado and Cavalca [28]. In this procedure, the fluid-film is discretized in a uniform mesh of finite volumes, as shown in Fig. 2a. In the close vicinity of the discontinuous film thickness, the pressure has an abrupt variation, and to compensate that, this pressure variation is attributed to a fluid velocity variation by writing a generalized Bernoulli equation immediately before and after the discontinuity (see [28] for more details).

Regarding the wear region, it is based on the geometry initial proposed by Dufrane et al. [29] and adapted by Machado and Cavalca [28], assuming abrasive wear. This model considers that the wear has a uniform thickness in axial direction; it can have a variable depth and can be located in any region of the bearing circumference.

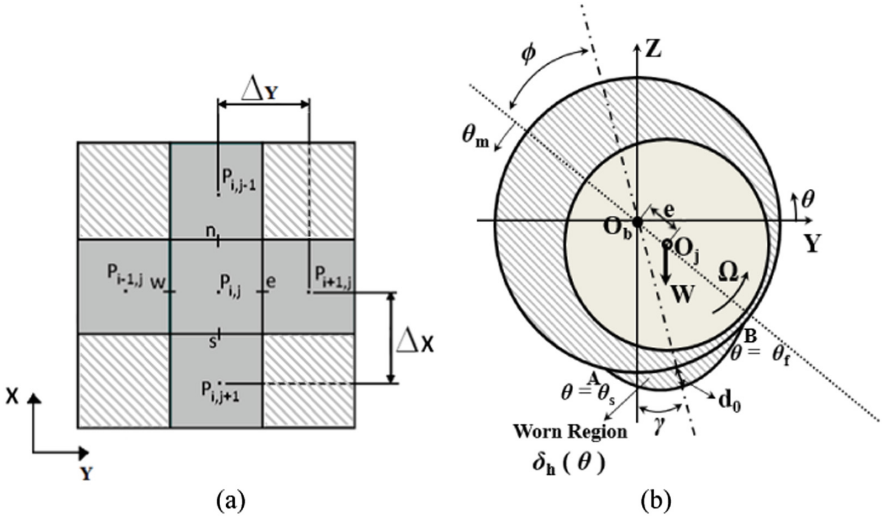

Fig. 2. Schematic representation: (a) finite volume mesh; (b) worn bearing geometry. (Adapted from Machado and Cavalca [28])

In the schematic draw of the worn bearing (Fig. 2b), it can be seen that the wear pattern introduces an additional oil layer with depth $\delta_h(\theta)$ in the region delimited by the angles θ_s and θ_f. Thus, the fluid-film thickness $h(\theta)$ in the presence of wear is given by Eq. (3), where $h_0(\theta)$ is the film thickness due to the shaft eccentricity.

$$h(\theta) = h_0(\theta) + \delta_h(\theta) \tag{3}$$

Equation (3) can also be written in the local reference system, denoted by θ_m in Fig. 2b:

$$\begin{aligned} h_0(\theta) &= Cr + e \cdot \cos(\theta_m) \\ \delta_h(\theta) &= d_0 - Cr \cdot (1 + \cos(\theta_m + \varphi)) \end{aligned} \tag{4}$$

Where Cr is the bearing radial clearance, e is the eccentricity of the shaft and d_0 is the maximum wear depth. Finally, the terms of Eq. (4) can be rewritten in the inertial reference system (Y, Z) through the eccentricity components e_y and e_z, respectively in the Y and Z coordinates:

$$\begin{aligned} h_0(\theta) &= Cr - e_z \cdot \cos(\theta - \pi/2) + e_y \cdot \sin(\theta - \pi/2) \\ \delta_h(\theta) &= d_0 - Cr \cdot (1 + \cos(\theta - \pi/2)) \end{aligned} \tag{5}$$

The depth $\delta_h(\theta)$ in the wear edges, $\theta = \theta_s$ and $\theta = \theta_f$, is zero. Consequently, the extreme points of wear are given by Eq. (6), where γ is the angular displacement of the center of wear, and the fluid-film thickness can be rewritten as Eq. (7).

$$\begin{aligned} \theta_s &= \pi/2 + \cos^{-1}(d_0/Cr - 1) + \gamma \\ \theta_f &= \pi/2 - \cos^{-1}(d_0/Cr - 1) + \gamma \end{aligned} \tag{6}$$

$$h(\theta) = \begin{cases} h_0, & 0 \le \theta \le \theta_s, \quad \theta_f \le \theta \le 2\pi \\ h_0 + \delta_h, & \theta_s < \theta < \theta_f \end{cases} \tag{7}$$

Equation (7) for the oil film thickness was then inserted into the Reynolds equation, which is solved using the finite volume method (see [28] for more details).

2.3 Model Reduction and Polynomial Approximation

Although the bearings coefficients come from a linearization of the Reynolds equation solution, they have a non-linear dependence on the rotational speed. Adding this variation to the system means that for each speed the system may present different linear (space-state) model. To control such system one possible strategy is to apply adapting controllers, which can variate according to a monitored parameter, e.g. the rotational speed. In this paper the adopted gain-scheduled control law requires describing the system in polynomial form. For that matter it is applied a least square second degree polynomial fit to approximate the dependence of each bearing coefficient to the rotational speed. The resultant bearing coefficients matrices can be described by Eq. (8). As a remark, most of the following polynomial formulation are depicted in second-degree but any degree would be applicable.

$$\begin{cases} \mathbf{K_{br}}(\boldsymbol{\Omega}) = \mathbf{K_{br0}} + \mathbf{K_{br1}}\boldsymbol{\Omega} + \mathbf{K_{br2}}\boldsymbol{\Omega}^2 \\ \mathbf{D_{br}}(\boldsymbol{\Omega}) = \mathbf{D_{br0}} + \mathbf{D_{br1}}\boldsymbol{\Omega} + \mathbf{D_{br2}}\boldsymbol{\Omega}^2 \end{cases} \tag{8}$$

The system is originally divided into 19 nodes, as in Fig. 1, of 4 degrees of freedom (DOF) each, totalizing 76 DOF. In space-state form the system has order 152, which is considerably high for LMI problems; therefore, reduction is necessary. Many reduction methods with different properties can be found in literature. Here is applied the Guyan reduction method [30], allowing to preserve the physical DOF, which makes easier to add the varying bearing coefficients based on the polynomial approximation and to include uncertainties, described in Sect. 3.2.

Firstly, the global matrices related to shaft, disc and journal are reduced using matrix **T** of Eq. (9) [30] preserving only the key nodes for the problem (4, 8, 12 and 16), which are the disc, journal and bearings. The resulting model has order 32, which is more suitable for LMI formulation. Moreover, since the bearings nodes DOF are preserved, the coefficients matrices from Eq. (8) can be directly added to the global reduced matrices. Thus, the space-state can be written as the matrix polynomial from Eq. (10). Note that the gyroscopic matrix can be inserted in the polynomial first degree term.

$$\begin{cases} \mathbf{M_{red}} = \mathbf{T}^T\mathbf{M_{fem}}\mathbf{T} \\ \mathbf{D_{red}} = \mathbf{T}^T\mathbf{D_{fem}}\mathbf{T} \end{cases} \quad \begin{cases} \mathbf{K_{red}} = \mathbf{T}^T\mathbf{K_{fem}}\mathbf{T} \\ \mathbf{K_{red}} = \mathbf{T}^T\mathbf{K_{fem}}\mathbf{T} \end{cases} \tag{9}$$

$$\dot{\mathbf{x}} = A(\boldsymbol{\Omega})\mathbf{x} + \mathbf{B}\mathbf{f} \tag{10}$$

Where,

$$\mathbf{A}(\Omega) = \mathbf{A_0} + \mathbf{A_1}\Omega + \mathbf{A_2}\Omega^2 = \begin{bmatrix} \mathbf{0} & \mathbf{I} \\ -\mathbf{M_{red}^{-1}}(\mathbf{K_{red}} + \mathbf{K_{br0}}) & -\mathbf{M_{red}^{-1}}(\mathbf{D_{red}} + \mathbf{D_{br0}}) \end{bmatrix} + \begin{bmatrix} \mathbf{0} & \mathbf{I} \\ -\mathbf{M_{red}^{-1}}\mathbf{K_{br1}} & -\mathbf{M_{red}^{-1}}(\mathbf{G_{red}} + \mathbf{D_{br1}}) \end{bmatrix}\Omega + \begin{bmatrix} \mathbf{0} & \mathbf{I} \\ -\mathbf{M_{red}^{-1}}\mathbf{K_{br2}} & -\mathbf{M_{red}^{-1}}\mathbf{D_{br2}} \end{bmatrix}\Omega^2$$

To facilitate the formulation of the controller it is possible to normalize the varying parameter as a unitary simplex Λ_2, Eq. (11).

$$\begin{aligned} &\mathbf{A}(\Omega) = \mathbf{A}(\alpha) = \mathbf{Ap_0} + \mathbf{Ap_1}\alpha_1 + \mathbf{Ap_2}\alpha_1^2 = \\ &\left[\mathbf{A_0} + \mathbf{A_1}a + \mathbf{A_2}a^2\right] + [\mathbf{A_1}(b-a) + \mathbf{A_2}2a(b-a)]\alpha_1 + \left[\mathbf{A_2}(b-a)^2\right]\alpha_1^2 \end{aligned} \tag{11}$$

Where,

$\alpha = \Lambda_2 \Leftrightarrow \sum_{n=1}^{2} \alpha_n, \alpha_n \geq 0$ and $\alpha_1 = \frac{\Omega - a}{b-a}$

a, b: minimum and maximum parameter variation, in this case, minimum and maximum rotational speed, respectively.

An important step to make the control design less conservative is to homogenize the polynomial, that is, making every term dependent on the same degree to the varying parameter. That can be done by using the unitary simplex property as in Eq. (12).

$$\begin{aligned} &\mathbf{A}(\alpha) = \mathbf{Ap_0}(\alpha_1 + \alpha_2)^2 + \mathbf{Ap_1}\alpha_1(\alpha_1 + \alpha_2) + \mathbf{Ap_2}\alpha_1^2 = \\ &\mathbf{Ap_{20}}\alpha_1^2 + \mathbf{Ap_{11}}\alpha_1\alpha_2 + \mathbf{Ap_{02}}\alpha_2^2 = \\ &[\mathbf{Ap_0} + \mathbf{Ap_1} + \mathbf{Ap_2}]\alpha_1^2 + [2\mathbf{Ap_0} + \mathbf{Ap_1}]\alpha_1\alpha_2 + \mathbf{Ap_0}\alpha_2^2 \end{aligned} \tag{12}$$

3 Control Formulation

3.1 Two-Stage Static Gain-Scheduled H_∞ Controller

Designing regulator H_∞ controllers generally follows a well-known framework [21, 31]. Firstly, an augmented plant, Eq. (13), based on state-space formulation, Eq. (10), is created separating the inputs in exogenous disturbances **w** and control signal **u**; and the outputs in performance signal **z**, usually composed by the actual objective (in this case disc displacement) and the control effort **u**, and the feedback signal **y**, which in most cases are the sensors readings.

$$\begin{cases} \dot{\mathbf{x}} = Ax + B_1\mathbf{w} + \mathbf{B_2u} \\ \mathbf{z} = \mathbf{C_1} + \mathbf{D_{11}w} + \mathbf{D_{12}u} \\ \mathbf{y} = \mathbf{C_2} + \mathbf{D_{21}w} + \mathbf{D_{22}u} \end{cases} . \qquad \mathbf{u} = \mathbf{Ly} \tag{13}$$

There are many structures and methods for solving the H_∞ control problem. However, the majority relies on linear time invariant systems, which may not be applicable for rotating machinery since their dynamics are strongly dependent on the rotational speed. Since considering the whole possible variations as uncertainties might be excessively conservative, a very usual solution has been applying gain-scheduled techniques. This way, the control law $\mathbf{L}(\alpha)$ also variates according to the current operation condition. In this paper, to obtain $\mathbf{L}(\alpha)$ dependent on Ω, the two-stage technique proposed by Agulhari [26] is applied. The method is based on Lyapunov quadratic stability and consists on solving two consecutive linear matrix inequalities (LMI) as described by Theorems 1 and 2, respectively. The resulting control has guaranteed Lyapunov stability for the considered conditions and presents no dynamic part, being an attractive option for real-time applications.

Theorem 1. There is a state-feedback gain $\mathbf{K}(\alpha) = \mathbf{Z}(\alpha)\mathbf{X}^{-1}$that stabilizes the system from Eq. (14), with $\mathbf{x} \in \mathbb{R}^n$ and $\mathbf{B_2} \in \mathbb{R}^{n,ic}$, if there are $\mathbf{P}(\alpha) = \mathbf{P}^T(\alpha) > 0 \in \mathbb{R}^{n,n}$, $\mathbf{X} \in \mathbb{R}^{n,n}$, $\mathbf{Z} \in \mathbb{R}^{ic,n}$ for a given $\xi > 0 \in \mathbb{R}$ which fulfill the LMI from Eq. (15).

$$\dot{\mathbf{x}} = (\mathbf{A}(\alpha) + \mathbf{B_2K}(\alpha))\mathrm{x} + \mathbf{B_1w} \tag{14}$$

$$\begin{bmatrix} \mathbf{A}(\alpha)\mathbf{X} + \mathbf{X}^*\mathbf{A}(\alpha)^* + \mathbf{B_2Z}(\alpha) + \mathbf{Z}(\alpha)^*\mathbf{B_2^*} & \mathbf{P}(\alpha) - \mathbf{X}^* + \xi\mathbf{A}(\alpha)\mathbf{X} + \xi\mathbf{B_2Z}(\alpha) \\ * & -\xi\mathbf{X} - \xi\mathbf{X}^* \end{bmatrix} < \mathbf{0} \tag{15}$$

*: Conjugate transpose.

The proof for the Theorem 1 can be found in [32].

Theorem 2. There exists an output-feedback control gain $\mathbf{L}(\alpha) = \mathbf{H}^{-1}\mathbf{J}(\alpha)$ that stabilizes the system from Eq. (16) and minimizes it's H_∞ norm, with $\mathbf{x} \in \mathbb{R}^n$, $\mathbf{w} \in \mathbb{R}^i$, $\mathbf{B_2} \in$

$\mathbb{R}^{ic}$, $\mathbf{C_2} \in \mathbb{R}^{oc,n}$, if there are $\mathbf{P}(\alpha) = \mathbf{P}^T(\alpha) > 0 \in \mathbb{R}^{n,n}$, $\mathbf{K}(\alpha) \in \mathbb{R}^{ic,n}$, $\mathbf{F}(\alpha) \in \mathbb{R}^{n,n}$, $\mathbf{G}(\alpha) \in \mathbb{R}^{n,n}$, $\mathbf{H} \in \mathbb{R}^{ic,ic}$, $\mathbf{J}(\alpha) \in \mathbb{R}^{ic,oc}$ and $\mu > \gamma^2 > 0 \in \mathbb{R}$ that fulfill the conditions in Eq. (17).

$$\begin{cases} \dot{\mathbf{x}} = (\mathbf{A}(\alpha) + \mathbf{B_2}\mathbf{L}(\alpha)\mathbf{C_2})\mathbf{x} + \mathbf{B_1}\mathbf{w} \\ \mathbf{z} = (\mathbf{C_1} + \mathbf{D_{12}}\mathbf{L}(\alpha)\mathbf{C_2})\mathbf{x} \end{cases} = \begin{cases} \dot{\mathbf{x}} = \mathbf{A_{CL}}(\alpha)\mathbf{x} + \mathbf{B_{CL}}\mathbf{w} \\ \mathbf{z} = \mathbf{C_{CL}}(\alpha)\mathbf{x} \end{cases} \tag{16}$$

$$\inf \left(\mu : \begin{bmatrix} \boldsymbol{\Psi_{11}} & \boldsymbol{\Psi_{12}} & \boldsymbol{\Psi_{13}} & \boldsymbol{\Psi_{14}} & \boldsymbol{\Psi_{15}} \\ & -\mathbf{G}(\alpha) - \mathbf{G}(\alpha)' & \mathbf{G}(\alpha)\mathbf{B_1} & \mathbf{0} & \mathbf{G}(\alpha)\mathbf{B_2} \\ & & -\mathbf{I} & \mathbf{0} & \mathbf{0} \\ & & & -\mu\mathbf{I} & \mathbf{0} \\ * & & & & -\mathbf{H} - \mathbf{H}' \end{bmatrix} < \mathbf{0} \right) \tag{17}$$

Where,

$$\boldsymbol{\Psi_{11}} = \mathbf{A}^T(\alpha)\mathbf{F}^T(\alpha) + \mathbf{F}(\alpha)\mathbf{A}(\alpha) + \mathbf{K}^T(\alpha)\mathbf{B}_2^T\mathbf{F}^T(\alpha) + \mathbf{F}(\alpha)\mathbf{B_2}\mathbf{K}(\alpha)$$

$$\boldsymbol{\Psi_{12}} = \mathbf{P}(\alpha) - \mathbf{F}(\alpha) + \mathbf{A}^T(\alpha)\mathbf{G}^T(\alpha) + \mathbf{K}^T(\alpha)\mathbf{B}_2^T\mathbf{G}^T(\alpha) \qquad \boldsymbol{\Psi_{13}} = \mathbf{F}(\alpha)\mathbf{B}_1^T$$

$$\boldsymbol{\Psi_{14}} = \mathbf{C}_1^T + \mathbf{K}(\alpha)^{\mathrm{T}}\mathbf{D}_{12}^T \qquad \boldsymbol{\Psi_{15}} = \mathbf{F}(\alpha)\mathbf{B_2} + \mathbf{C}_2^T\mathbf{J}(\alpha)^T - \mathbf{K}^T(\alpha)\mathbf{H}^T$$

The proof for the Theorem 2 can be found in [26].

The conditions for the second stage, Eq. (17), are not linear since there are terms with two variable product ($\mathbf{K}(\alpha)$ and $\mathbf{F}(\alpha)$). In the proof of Theorem 2, one arrives at a condition where $\mathbf{K}(\alpha)$ is a stabilizing state-feedback gain. Thus, it is possible to utilize the first stage to generate generic gains $\mathbf{K}(\alpha)$ and apply it as a constant in the second-stage. Due to this linearization the method presents only a sufficient condition, that is, if no solution can be found doesn't mean it does not exist. Moreover, since it is also difficult to find a correlation between the first stage and the final performance, Agulhari et al. [32] propose testing different solutions for $\mathbf{K}(\alpha)$ (through the variation of ξ) to increase the chance of finding better results. Therefore, any other LMI condition that generates stabilizing gain would be fitting as a first stage.

3.2 Uncertainties

The problem of deviation from a linear time invariant model due to rotational speed variation is addressed by the gain-scheduled method. However, the problem of bearing wear presents a challenging approach, since it may be difficult to parametrize it during the machine operation. Although abrasive wear usually occurs gradually and is not as evident as variations due to rotational speed, it can reach levels in which the system dynamic is too distant from the nominal condition and, if not taken into account, may result in serious performance loss or even instability in close-loop. To address the effect of bearing wear, here it is proposed to include the possible variations, limited to a certain range, as structured uncertainties.

Supposing the uncertain bearings parameters Δp follows the model from Eq. (18), where the effect of the abrasion depth is expressed by the linear approximation δ_d and the rotational speed influence is expressed by the polynomial in $\boldsymbol{\Omega}$, as in Sect. 2.3. The state-space matrix $\mathbf{A}$ becomes the uncertain matrix $\mathbf{A_{unc}}$, Eq. (19), where $\boldsymbol{\Delta K}$ and $\boldsymbol{\Delta C}$ are the uncertain bearing coefficients matrices composed by the terms from Eq. (18).

$$\Delta p_{jk} = p_{jk} + \delta_d \left(p_{jk2} \Omega^2 + p_{jk1} \Omega + p_{jk0} \right) \tag{18}$$

Where,

$$p = (k, d),\ j \text{ and } j \text{ and } k = (y, z).$$

$$\mathbf{A_{unc}}(\alpha) = \mathbf{A}(\alpha) + \begin{bmatrix} \mathbf{0} & \mathbf{I} \\ -\mathbf{M_r^{-1}} \boldsymbol{\Delta K}(\Omega, \delta_d) & -\mathbf{M_r^{-1}} \boldsymbol{\Delta D}(\Omega, \delta_d) \end{bmatrix} \tag{19}$$

It is possible to extract the uncertainties from $\mathbf{A_{unc}}$ obtaining the augmented system from Eq. (20) with the auxiliary input ($\mathbf{h}$), output ($\mathbf{g}$) and structured uncertain matrix $\boldsymbol{\Delta}$. Note that since the uncertainties are dependent on the rotational speed, $\mathbf{B_u}$ is dependent on $\boldsymbol{\Omega}$ and can also be easily written in terms of α and homogenized. This augmented plant can be used as base for synthetizing robust controllers or analyzing robust stability. For example, if the H_∞ norm from $\mathbf{h}$ to $\mathbf{g}$ is smaller than one, the system is guaranteed to be stable for any possible considered uncertainty by the small gain theorem [31]. Even though the applied control in this paper focus on reducing the H_∞ norm, utilizing this metric for robust analysis may offer very conservative analysis. Therefore, it is proposed to apply μ-analysis [13, 23, 33] to evaluate the systems robustness.

$$\begin{cases} \dot{\mathbf{x}} = A(\alpha)\mathbf{x} + \mathbf{B_u}(\boldsymbol{\Omega})\mathbf{h} + \mathbf{B_1}\mathbf{w} + \mathrm{B_2}\mathbf{u} \\ \mathbf{g} = \mathbf{C_u}\mathbf{x} \\ \mathbf{z} = \mathbf{C_1}\mathbf{x} + \mathbf{D_{12}}\mathbf{u} \\ \mathbf{y} = \mathbf{C_2}\mathbf{x} \\ \mathbf{u} = \mathbf{L}(\alpha)\mathbf{y} \\ \mathbf{h} = \Delta\mathbf{g} \end{cases} \tag{20}$$

3.3 Controllers and Weighting Filters

In this paper two controllers are compared: $\mathbf{L}$ and $\mathbf{Lu}$ are respectively static H_∞ gain-scheduled controller without and with uncertainties. That is, both are obtaining solving the two-stage LMIs from Sect. 3.1, however, $\mathbf{Lu}$ also includes $\mathbf{h}$ in the inputs and $\mathbf{g}$ in the outputs. For $\mathbf{Lu}$ the matrix $\mathbf{B_1}$ will be concatenated with $\mathbf{B_u}$ and written as a polynomial in α. The resultant $\mathbf{B_1}(\alpha)$ can be applied to the two-stage method without any loss of generality.

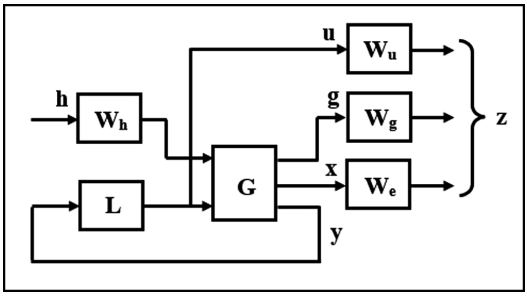

Fig. 3. Weighting filters

The final performance and feasibility of MIMO H_∞ are strongly related to weighting filters. They are functions that adjust the scale and priority between the outputs and inputs. Here are applied the filters according to Fig. 3 and Eq. (21).

$$\mathbf{W_e}(s) = \left(\frac{s}{\sqrt[k]{M_e}} + \omega \over s + \sqrt[k]{\varepsilon_e}\omega\right)^k \quad \mathbf{W_u}(s) = g_u\left(\frac{s + \frac{\omega}{\sqrt[k]{M_u}}}{\sqrt[k]{\varepsilon_u}s + \omega}\right)^k \quad \mathbf{W_h} = \mathbf{W_g} = g_h \tag{21}$$

4 Results

The controllers' synthesis and simulations for the rotor described in Sect. 2 are done considering the frequency range from 20 to 100 Hz, an abrasive wear depth varying from 0 to 40 μm at 20° at the second bearing, and an unbalance momentum of 1×10^{-4} kg.m. The bearings coefficients are calculated as described in Sect. 2.2 and then approximated by a second order polynomial fit. For the **Lu** gain and μ-analysis, the bearing 2 coefficient is considered to be the mean value between the parameters without damage and 40 μm wear depth. And the polynomial regarding the uncertain is fitted to represent the difference between the mean and the nominal value, allowing the uncertain $\delta \in [-1,1]$ to cover most of the possible variations. The control gains are obtained in Matlab® using the ROLMIP package [34] to formulate and automatic homogenize the problem and the solver SDPT-3 [35].

The dynamic related to the magnetic actuator is neglected since it is usually much faster than the mechanical response, also no unity conversions are considered, therefore the control gains represent a direct relation between the bearings displacement readings (in meters) and control force (in Newtons).

This result section is organized starting by the polynomial approximation, followed by the utilized control parameters and final structures, then the system robustness is analyzed by means of μ norm, and finally, the achieved performance for each controller is compared.

4.1 Bearing Coefficients Approximation

The influence of different abrasive wear depth on the bearings parameters is shown in Fig. 4a. It is possible to notice that they have a non-linear behavior, therefore the adopted linear approximation for the depth uncertain may lack precision. One could try to express each parameter as an independent uncertainty. However, it would generate an excessively conservative result, since it would comprehend combinations between parameters related to different wear degrees for the same bearing.

The first step to design the controllers is finding the polynomial fit for the bearings coefficients which will be used to design the gain-scheduled controllers. Figure 4b shows the second order approximation for the first bearing stiffness utilized for both **L** and **Lu**. For the damping and the second bearing coefficients similar results are obtained. However, for **Lu** and μ-analysis the polynomial approximations for the second bearing are regarding the mean parametrical variation value, as explained before. Figure 4a shows the considered mean, and polynomial approximation for the second bearing stiffness uncertainty.

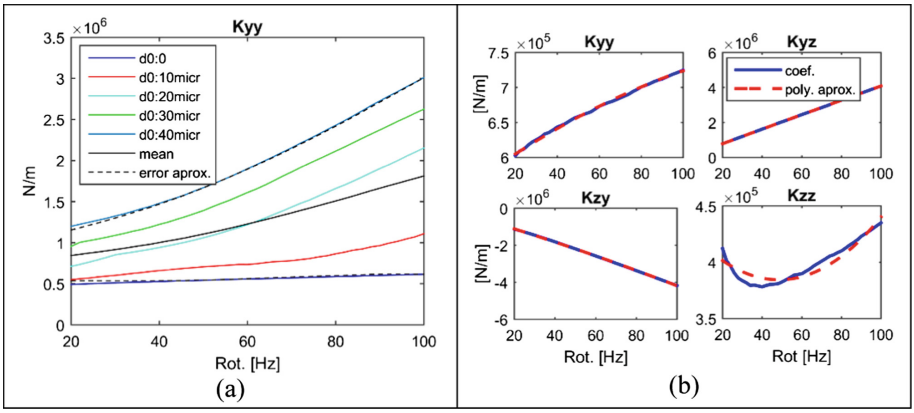

Fig. 4. (a) Bearing number 2 stiffness coefficient for different abrasive wear depths, utilized mean and second order polynomial error bounds. (b) Bearing number 1 stiffness coefficients and second degree polynomial approximation.

4.2 Control Parameters

As stated before, the weighting functions have strong relation to the final control performance. This section brings the utilized weighting parameters, Table 1. The weighting functions for **L** was adjusted aiming the maximum vibration attenuation at nominal condition. For **Lu** the adjustment also considered maintaining the resultant μ norm bellow one. It is important to remark that these configurations are suboptimum, since, as explained in Sect. 3.2, loss of necessity occurs. The final control function **Lu** is given by Eq. (22), and **L** follows the same structure. Note that the final **L** and **Lu**

control expressions consist in gains obtained by a weighted sum between matrices, which can be done without problems in real time.

$$\mathbf{Lu}(\alpha) = 10^6 \begin{bmatrix} -0.1909 & 2.3607 & -0.0822 & 0.0258 \\ -2.3272 & 0.1948 & -0.0359 & -0.0777 \end{bmatrix} \alpha_1 + 10^6 \begin{bmatrix} 0.1246 & 1.8734 & -0.0279 & 0.0076 \\ -2.0348 & 0.7281 & -0.0280 & -0.0117 \end{bmatrix} (1 - \alpha_1) \quad (22)$$

Table 1. Control parameters

	ω (Hz)	k	M_u	M_e	ε_u	ε_e	g_u	g_h
L	220	4	1	100	0.1	1	$2{\cdot}10^{-6}$	–
Lu	220	4	1	100	0.1	1	$5{\cdot}10^{-5}$	$4{\cdot}10^{-3}$

4.3 Robustness Analysis

To evaluate the robustness level of the systems the peak μ value for a set of speeds between 20 and 100 Hz is calculated and displayed in Fig. 5. Where OL is the open-loop system, and CL and CLu are the closed loops with **L** and **Lu**, respectively.

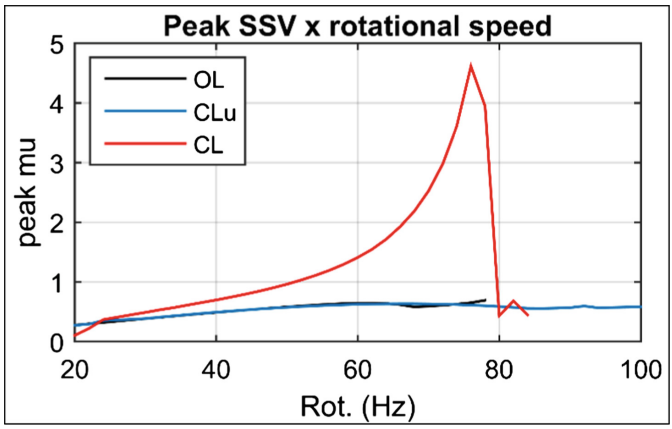

Fig. 5. μ-peak diagram.

Analyzing Fig. 5 it is possible to observe that the open-loop system does not crosses one, therefore the bearing wear, in the considered range, is not expected to affect the system stability. However, it is expected instability near 80 Hz (line interruption when reaching eigenvalue positive real part), due to fluid-induced instability. For the **Lu** closed-loop the bearing wear is also expected to not destabilize the system, moreover, the fluid-induced instability is suppressed for the whole considered rotational speed range (continuous line). As for **L**, although in the diagram the line is

interrupted near 84 Hz suggesting that the controller cannot stabilize fluid-induced instability, it is important to remind that this diagram is based on the mean value for bearing number two (Fig. 4a), i.e. the system is not the nominal one. Therefore, it is expected some level of discrepancy. However, the analysis for the μ-value still holds, and since the line crosses 1, that indicates that **L** does not guarantee stability when dealing with wear conditions.

4.4 Unbalance Response

To perform the unbalance response analysis a set of systems at different rotational speed for the nominal condition and 40 μm at 20° wear were generated. Their eigenvalue and frequency response at each respective speed were analyzed to define if the system is stable and what is the maximum amplitude of the orbit. The results for the responses at the bearing number 2 node are shown in Fig. 6 and Table 2. It is possible to notice the nominal **OL** system presents its peak response near 45.9 Hz (critical speed), and instability at 79.2 Hz. It is interesting to observe that, as predicted in μ-analysis, the considered bearing wear does not cause the system instability to be anticipated but rather delayed to 81.6 Hz. However, it did cause a fairly amplification on the vibration level. As for the **Lu** controller, it manages to considerably attenuate the vibration level and, as expected by the μ-analysis, also guarantee stability for the whole frequency range even with damaged bearing. Regarding the **L** controller, it does stabilize the system and reduces the vibration peak for the nominal condition, but under wear effects, it may lead the system to instability even before the nominal fluid-induced threshold (60.7 Hz).

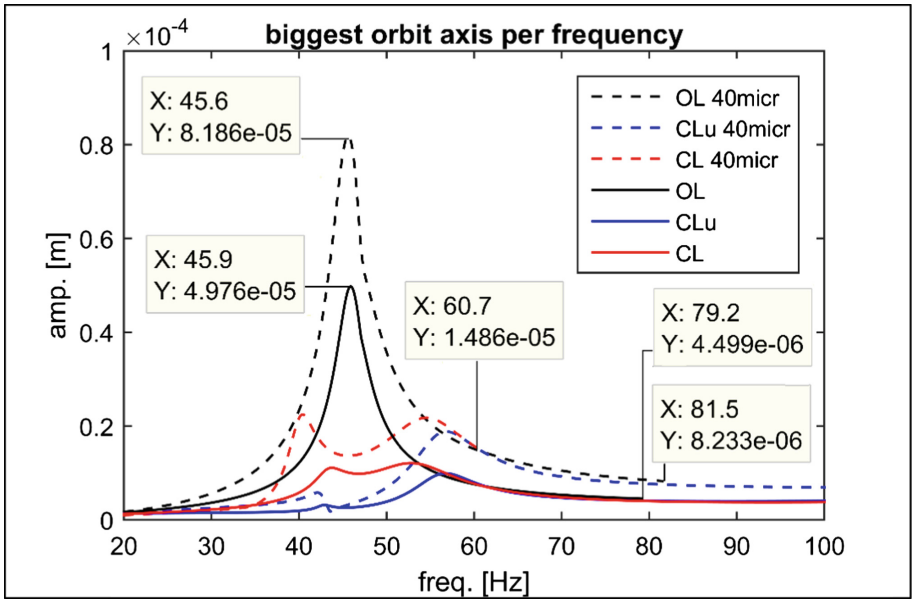

Fig. 6. Unbalance response at bearing number 2 for 0 and 40 μm depth.

Table 2. Main unbalance response parameters

Depth 0/40 μm	Peak freq. [Hz]	Peak amp. (μm)	Instab. freq. [Hz]
OL	45.9/45.6	49.76/81.86	79.2/81.5
CLu	56.4/56.8	9.83/18.81	–
CL	52.8/54.5	12.05/21.76	–/60.7

5 Conclusion

In this preliminary study about the wear effects of bearing wear on active controlled systems it was possible to observe that in open-loop condition, although the wear, for the considered range, does not destabilize the system, it does amplify the vibration levels in the bearing, which could lead to damage propagation. When in closed-loop, the vibration amplitude can be significantly attenuated, but stability can be critically compromised if the coefficients variation is not accounted for. To perform the robustness analysis and to synthetize a robust controller an uncertain model was proposed considering a linear approximation for the depth influence. Although the results were promising, accurately accusing instability risks due to bearing damage for CL while predicting stability for OL and CLu, further analysis is to be conducted to verify this approximation precision. If necessary, other degrees or other parameters may be included in the uncertain model providing a more accurate model in exchange for more computational requirements.

Acknowledgements. The authors would like to thank CAPES, CNPq and Grants # 2015/20363-6, # 2016/13059-1 and # 2017/07454-8 from the São Paulo Research Foundation (FAPESP) for the financial support to this research.

References

1. Suzuki, K., Tanaka, M.: Stability characteristics of worn journal bearing. In: Proceedings of the Asia-Pacific Vibration Conference, Kuala Lumpur, pp. 296–301 (1995)
2. Kumar, A., Mishra, S.: Stability of a rigid rotor in turbulent hydrodynamic worn journal bearings. Wear **193**, 25–30 (1996)
3. Bouyer, J.M., Fillon, M., Pierre-Danos, I.: Influence of wear on the behavior of a two-lobe hydrodynamic journal bearing subjected to numerous start-ups and stops. J. Tribol. **129**, 205–208 (2007)
4. Muzakkir, S.M., Hirani, H., Thakre, G.D.: Experimental investigations on effectiveness of axial and circumferential grooves in minimizing wear of journal bearing operating in mixed lubrication regime. Int. J. Curr. Eng. Technol. **5**, 486–489 (2015)
5. Machado, T.H., Mendes, R.U., Cavalca, K.L.: Directional frequency response applied to wear parameter identification in hydrodynamic bearings. Mech. Res. Commun. **74**, 60–71 (2016)
6. Okac, H., Loparo, K.A., Discenzo, F.M.: Online tracking of bearing wear using wavelet packet decomposition and probabilistic modeling: a method for bearing prognostics. J. Sound Vib. **302**, 951–961 (2007)

7. Wu, T., Mao, J., Dong, G., Xu, H., Xie, Y.: Journal bearing wear monitoring via on-line visual ferrograph. Adv. Mater. Res. **44**, 189–194 (2008)
8. Chasalevris, A.C., Nikolakopoulos, P.G., Papadopoulos, C.A.: Dynamic effect of bearing wear on rotor-bearing system response. ASME J. Vib. Acoust. **135**(1), 011008–011008-12 (2013)
9. Papadopoulos, C.A., Nikolakopoulos, P.G., Gounaris, G.D.: Identification of clearances and stability analysis for a rotor-journal bearing system. Mech. Mach. Theory **43**, 411–426 (2008)
10. Machado, T.H., Cavalca, K.L.: Geometric discontinuities identification in hydrodynamic bearings. In: Proceedings of 9th IFToMM International Conference on Rotor Dynamics, vol. 1, pp. 1–10. Politecnico di Milano, Milan, Italy (2014)
11. Siqueira, A.A.G., Nicoletti, R., Norrick, N., Cavalca, K.L., Castro, H.F., Bauer, J., Dohnal, F.: Linear parameters varying control desing for rotating systems supported by journal bearings. Elsevier J. Sound Vib. **331**, 2220–2222 (2012)
12. Fittro, R.L., Knospe, C.R.: Rotor compliance minimization via mu-control of active magnetic bearings. IEEE Trans. Control Syst. Technol. **10**, 238–249 (2002)
13. Riemann, B., Sehr, M.A., Schittenhelm, R.S., Rinderknecht, S.: Real gyroscopic uncertainties in robust control of flexible rotors. In: Proceedings of the IEEE Conference on Decision and Control, pp. 3762–3769 (2013)
14. Riemann, B., Sehr, M.A., Schittenhelm, R.S., Rinderknecht, S.: Robust Control of Flexible High-Speed Rotors Via Mixed Uncertainties, pp. 2343–2350 (2013)
15. Schittenhelm, R.S., Rinderknecht, S.: Controllers for Attenuation of Lateral Rotor Vibration Part I: Controller Design, pp. 1753–1762 (2015)
16. Schittenhelm, R.S., Rinderknecht, S.: Controllers for Attenuation of Lateral Rotor Vibration Part II: Controller Optimization and Comparison, pp. 1763–1773 (2015)
17. Becker, F.B., Sehr, M.A., Rinderknecht, S.: Vibration isolation for parameter-varying rotor systems using piezoelectric actuators and gain-scheduled control. J. Intel. Mater. Syst. Struct. **28**(16), 1–12 (2017)
18. Dimitri, A.S., El-Shafei, A., Adly, A.A., Mahfoud, J.: Magnetic actuator control of oil whip instability in bearings. IEEE Trans. Magn. **51**, 1–4 (2015)
19. Riemann, B., Perini, E.A., Cavalca, K.L., Castro, H.F., Rinderknecht, S.: Oil whip instability control using μ-synthesis technique on a magnetic actuator. Elsevier J. Sound Vib. **332**, 654–673 (2013)
20. Wu, M.F., Mendes, R.U., Cavalca, K.L.: Vibration control of a journal-bearing supported rotor using gain-scheduled controller via LMI. In: Proceedings of the XVII International Symposium on Dynamic Problems of Mechanics, pp. 1–10 (2017)
21. Schweitzer, G., Maslen, E.H.: Magnetic Bearings. Springer, Berlin (2009)
22. Balini, H.M.N.K., Witte, J., Scherer, C.W.: Synthesis and implementation of gain-scheduling and LPV controllers for an AMB system. Automatica **48**, 521–527 (2012)
23. Kuseyri, İ.S.: Robust control and unbalance compensation of rotor/active magnetic bearing systems. J. Vib. Control **18**, 817–832 (2012)
24. Yu, J., Zhu, C.: A Sensor-fault tolerant control method of active magnetic bearing in flywheel energy storage system. In: IEEE Vehicle Power and Propulsion Conference (VPPC), pp. 1–6 (2016)
25. Gouws, R., Schoor, G.: A comparative study of fault detection and correction techniques on active magnetic bearing systems. In: IEEE, pp. 1–10 (2007)
26. Agulhari, C.M., Oliveira, R.C.L.F., Peres, P.L.D.: Static output feedback control of polytopic systems using polynomial Lyapunov functions. IEEE Conf. Decis. Control **49**, 6894–6901 (2010)

27. Nelson, H.D., Mcvaugh, J.M.: The dynamics of rotor-bearing systems using finite elements. J. Eng. Ind. **98**, 593–600 (1976)
28. Machado, T.H., Cavalca, K.L.: Modelling of hydrodynamic bearing wear in rotor-bearing systems. Mech. Res. Commun. **69**, 15–23 (2015)
29. Dufrane, K.F., Kannel, J.W., McCloskey, T.H.: Wear of steam turbine journal bearings at low operating speeds. J. Lubr. Technol. **105**, 313–317 (1983)
30. Guyan, R.J.: Reduction of stiffness and mass matrices. AIAA J. **3**, 380 (1965)
31. Zhou, K.: Essentials of robust control. Prentice Hall, New York (1998)
32. Agulhari, C.M., Oliveira, R.C.L.F., Peres, P.L.D.: LMI relaxations for reduced-order robust H ∞ control of continuous-time uncertain linear systems. IEEE Trans. Autom. Control **57**, 1532–1537 (2012)
33. Doyle, J., Wall, J., Stein, G.: Performance and robustness analysis for structured uncertainty. In: 21st IEEE Conference on Decision and Control, pp. 629–636 (1982)
34. Oliveira, R.C.L.F., Peres, P.L.D.: Parameter-dependent LMIs in robust analysis: characterization of homogeneous polynomially parameter-dependent solutions via LMI relaxations. IEEE Trans. Autom. Control **52**, 1334–1340 (2007)
35. Toh, K.C., Todd, M.J., Tutuncu, R.H.: SDPT3—a Matlab Software Package for Semidefinite Programming. Optimization Methods and Software **11**, 545–581 (1999)